JOURNAL OF CATALYSIS 133, 231–246 (1992)

Preparation and Characterization of Nickel–Aluminum Mixed Oxides Obtained by Thermal Decomposition of Hydrotalcite-Type Precursors

O. CLAUSE,*,[1] B. REBOURS,* E. MERLEN,* F. TRIFIRÓ,† AND A. VACCARI†

*Institut Français du Pétrole, 1 Avenue de Bois-Préau BP 311, 92506 Rueil-Malmaison, France; and †Dipartimento di Chimica Industriale e dei Materiali, Viale Del Risorgimento 4, 40136 Bologna, Italy

Received June 17, 1991; revised August 12, 1992

A series of nickel–aluminum mixed hydroxides was prepared by coprecipitation and their structure and composition was examined by X-ray diffraction and thermal analysis. The homogeneity of the Ni(II) and Al(III) cations in the brucite-type layers has been verified by EXAFS spectroscopy. The hydrotalcite-type precipitates were calcined and the composition of the resulting mixed oxides investigated. The selective dissolution of a Ni-doped alumina phase has been performed in concentrated NaOH solution. The alumina phase significantly contributes to the surface area of the mixed oxides but is suggested to play a minor role for the thermal stability of nickel oxide. A model for the nickel–aluminum mixed oxides obtained from hydrotalcite decomposition is proposed to involve the formation of nickel oxide and Ni-doped alumina phases in strong interaction with partially decomposed precursor layers or with a spinal-type phase at the $NiO-Al_2O_3$ interface. The latter phase is thought to be responsible for the thermal stabilization of the nickel oxide phase. © 1992 Academic Press, Inc.

INTRODUCTION

Hydrotalcite-type anionic clays are currently used as precursors for aldol condensation and epoxide polymerization (*1–3*), hydrogenation (*4–7*), and steam-reforming catalysts (*8–10*). The nickel–aluminum mixed oxides resulting from the thermal decomposition of hydrotalcite-like coprecipitates are among the most studied catalysts precursors for steam-reforming and methanation reactions. The interest in these oxides is due to remarkable properties of the final catalysts, such as a high metallic dispersion and a high particle stability against sintering under extreme conditions for nickel contents up to 75 wt% (*11–17*). Two models have been proposed to explain the origin of the stability of the nickel particles after reduction. The nucleation of an alumina phase on the surface of the nickel crystallites as reduction proceeds has been proposed (*13*). This nucleation was thought to occur by diffusion of aluminum ions from the bulk of the nickel oxide particles. The alumina phase, together with a Ni-doped alumina formed during calcination, was considered as a support in intimate contact with the nickel particles preventing particle sintering. This model was supported by an electron microscopy investigation of the catalysts after extraction of nickel as nickel carbonyl (*18*). This study showed a porous, sponge-like structure, likely alumina, with a mesoporosity in which the nickel particles were trapped before extraction.

In a second model, the nickel particles obtained by reduction of the calcined hydrotalcite precursors have been suggested to be "paracrystalline," the lattice of the nickel particles being strained by defects consisting of aluminate groups (*9*). The concept of paracrystallinity, first applied to ammonia synthesis catalysts (*19*), may be applicable to nickel catalysts. Using a very simple mathematical model, Schultz has demonstrated how homogeneously distributed $FeAl_2O_4$ point defects in an iron matrix

[1] To whom correspondence should be addressed.

0021-9517/92 $3.00
Copyright © 1992 by Academic Press, Inc.
All rights of reproduction in any form reserved.

(paracrystallinity) induced an equilibrium iron particle size (*20*). The paracrystallinity of nickel particles was justified on the basis that the complete removal of the aluminate groups from the nickel lattice during reduction would be energetically unfavorable. An original model of the Ni–Al oxide form named "continuously variable phase model" was also proposed (*9*).

The composition of the mixed oxides was relatively homogeneous and there was a continuous evolution from an Al-doped nickel oxide to a "spinel-like material" and finally to true spinel and nickel oxide phases with increasing calcination temperature. No alumina phase was detectable by X-ray diffraction independent of the calcination temperature. However, this model failed to explain the reasons for the thermal stability of the nickel oxide particles in the calcined state.

In this paper we have studied the thermal stability and reducibility of mixed oxides obtained from hydrotalcite-type precursors. The structure of the coprecipitates has been investigated by thermogravimetric analysis, X-ray diffraction, and EXAFS techniques to ensure that the coprecipitation operation does not induce heterogeneities such as separated phases of nickel hydroxide or aluminum hydroxide. The existence of an alumina phase in the calcined precursors is discussed in view of the loss of aluminum upon washing the solid with hot alkaline solutions, the nickel oxide being insoluble under these conditions. The thermal stability and reducibility of the washed mixed oxides have been examined. Finally, a new model for the calcined precursor involving the presence of a very stable compound at the nickel oxide–alumina interface is proposed. This model provides an explanation for the properties of the calcined precursors and the stability of the reduced catalysts.

EXPERIMENTAL

Hydrotalcite-type precursors were prepared by coprecipitation at pH 8.0 ± 0.1 by adding a solution of the nickel and aluminum nitrates to a solution containing a slight excess of $NaHCO_3$. The Ni/Al molar ratios in solution ranged from 0.3 to 3.0. The coprecipitates were kept in suspension at 60°C for 30 min under stirring then filtered and washed with distilled water at 60°C until Na_2O contents lower than 0.02% w/w were reached. The coprecipitates were then subjected to a hydrothermal treatment (200°C, 2.5 MPa, 48 h) using a Teflon-lined container so as to avoid the formation of nickel silicates (from glass). The materials were then dried overnight in an oven at 100°C.

The Ni and Al contents in the coprecipitates were determined by X-ray fluorescence spectroscopy. The precursors were calcined in air for 12 h at various temperatures ranging from 350 to 900°C. The calcined samples were subsequently treated with sodium hydroxide solutions as follows: suspensions of 0.2 g of sample suspended in 100 cm^3 of a 1 *N* sodium hydroxide solution were refluxed at 90°C under energetic stirring. The solutions were then filtered and the resulting materials rinsed with distilled water. The Ni(II) and Al(III) concentrations in the washing solutions and in the insoluble materials were determined by atomic absorption and X-ray fluorescence spectrometries, respectively. The alkaline treatments were performed in polyethylene containers so as to prevent glass dissolution leading to nickel silicate formation. Likewise, the washing solutions were kept in glass-free containers. The absence of silicon ions in the NaOH-treated products is of paramount importance: the formation of nickel silicates greatly modifies the thermal properties of nickel oxide, hindering the reduction and stabilizing the NiO particle dimensions.

The surface areas of the samples were determined on a Carlo Erba Sorptomatic Model 1700, using nitrogen adsorption.

X-ray powder diffraction analysis was carried out with a Phillips PW 1820 diffractometer using a cobalt target and a secondary beam monochromator. The wavelength was Co $K\alpha_{1,2}$ = 0.17209 nm. A $K\alpha_1$–$K\alpha_2$ deconvolution was performed before further

calculation on the XRD data. The lattice constants were determined by least-squares refinements. The nickel oxide crystallite size dimensions were obtained by the Scherrer equation averaging the values obtained from (111), (200), and (220) reflections using the Warren correction for instrumental broadening.

The temperature-programmed reduction profiles (TPR) of samples after various thermal treatments were obtained on a thermogravimetric device described previously (heating rate: 5°C/min) (*21*). The weight losses, due to the reaction $NiO + H_2 \rightleftharpoons Ni + H_2O$, were recorded as a function of temperature. Preliminary tests of water adsorption and desorption on calcined materials revealed that water was not adsorbed (or fully desorbed) at temperatures higher than 200°C.

EXAFS (extended X-ray absorption fine structure) measurements were performed at the LURE radiation synchrotron facility using the X-ray beam emitted by the DCI storage ring. The energy was scanned with 2-eV steps starting from 100 eV below until 600 eV above the Ni *K* absorption edge. A channel-cut single crystal of silicon was used as a monochromator. The edge jump heights (μx variation through the edge, x being the sample thickness) ranged from 0.8 to 1.2 for all samples and references. The analysis of the EXAFS spectra was performed following standard procedure for background removal, extraction of the EXAFS signal, and normalization to the edge adsorption. Fourier transforms of the EXAFS spectra were made after multiplication of the signal by a k^3 factor over a 3 to 12 $Å^{-1}$ Hanning window. The Hanning window was identical for the references and investigated systems. All fittings were performed both in *E* and *R* spaces.

Samples were examined by transmission electron microscopy using a Jeol 120 CX at 100 kV. Thin foils of the solids (about 70 nanometers in thickness) were obtained by ultramicrotomy using a diamond knife on grains embedded in an epoxy resin.

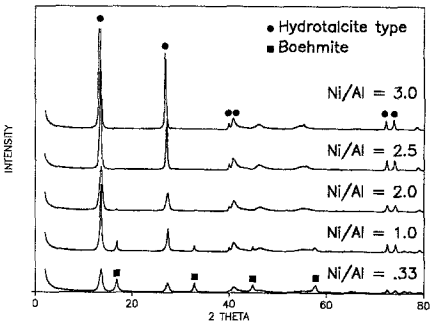

FIG. 1. XRD powder patterns of nickel–aluminum mixed hydroxides with different Ni/Al molar ratios after hydrothermal treatment.

RESULTS

Characterization of the Coprecipitates

The Ni/Al atomic ratios in the coprecipitates were determined by X-ray fluorescence and the results are reported in Table 1. The Ni/Al atomic ratios in solution before coprecipitation and in the mixed hydroxide precipitates are identical. Both Ni(II) and Al(III) ions quantitatively precipitate during preparation.

A well-crystallized hydrotalcite-type structure is present in all samples; see the X-ray diffraction patterns in Fig. 1. In addition to this structure, a boehmite-like aluminum oxyhydroxide phase is observed in the samples with a Ni/Al ratio below 2 (samples D and E). The hydrotalcite-type coprecipitates have a rhombohedral *R*-3 m symmetry. In the hydrotalcite-type structure, the Ni(II) and Al(III) cations are incorporated in brucite-type layers, the excess positive charge of the layers being compensated by carbonate ions in the interlayers (*22*). The *a* and *c* unit cell parameters (*c* corresponding to three times the distance between adjacent brucite-type layers) extracted from the XRD data, are presented in Table 2. The lattice constants obey Vegard's law in the Ni/Al molar ratio range $2 < Ni/Al < 3$ but are independent of the composition for Ni/Al ratios below 2, in accord with previous studies (*23*).

The TG–DTG diagrams of the samples in

TABLE 1

Chemical Composition of Samples A–E

Sample	Chemical analysis				Total weight loss (%) on thermal decomposition	Sample formulae
	Ni (wt%)	Al (wt%)	CO_3 (wt%)	Ni/Al molar ratio		
A	40.7	6.33	5.4	3.0	32.0	$[Ni_{0.75}Al_{0.25}(OH)_2](CO_3)_{0.12} \cdot 0.50\ H_2O$
B	39.7	7.37	6.8	2.5	32.3	$[Ni_{0.72}Al_{0.28}(OH)_2](CO_3)_{0.14} \cdot 0.54\ H_2O$
C	37.7	8.40	8.8	2.0	33.0	$[Ni_{0.67}Al_{0.33}(OH)_2](CO_3)_{0.16} \cdot 0.45\ H_2O$
D	30.3	13.8	7.8	1.0	32.4	Mixture of hydrotalcite and boehmite
E	18.7	26.1	n.d.	0.33	29.3	Mixture of hydrotalcite and boehmite

air are presented in Fig. 2. For samples A, B, C, corresponding to Ni/Al molar ratios between 2 and 3, two weight losses are detected: the first loss around 210°C may be attributed to interlayer water whereas the second one around 360°C is due to the dehydroxylation of the brucite-type layers and the elimination of carbonate ions from the interlayers (*22*). The weight losses relative to the weight of starting material and the sample formulae, deduced from X-ray fluorescence and thermal analysis, are shown in Table 1. In addition to the two weight losses at 210 and 360°C, samples D and E exhibit an additional weight loss at 260°C, indicating the presence of another phase in these samples. This weight loss increases with the aluminum content in the samples (see Fig. 2): the presence of an aluminum (oxy)hydroxide phase in samples D and E revealed by XRD is thus compatible with TG–DTG analysis.

TABLE 2

X-Ray Diffraction Data for Samples A–E

Sample	Ni/Al atomic ratio	Phases detected by XRD	Hydrotalcite structure lattice constants (nm)	
			a	*c*
A	3.0	Hydrotalcite-like	0.3041	2.317
B	2.5	Hydrotalcite-like	0.3035	2.293
C	2.0	Hydrotalcite-like	0.3027	2.272
D	1.0	Hydrotalcite-like + boehmite	0.3028	2.270
E	0.33	Hydrotalcite-like + boehmite	0.3028	2.273

The Fourier-transformed EXAFS spectra of samples A–E at the Ni *K* edge are presented in Fig. 3. The first peak from the origin of each spectrum is due to the first neighbors around the Ni(II) ions in the precipitates, i.e., oxygen atoms belonging to water molecules or OH groups. Amplitude and phase functions for the Ni–O system have been extracted from the spectrum of stoichiometric NiO and the composition of the first peak of sample A is given in Table 3. The composition of the first peak of samples A–E is visibly identical (see Fig. 3) and has been omitted for samples B–E. The coordination number is equal to 6.3 ± 1.0. Thus the Ni(II) ions maintain their octahedral coordination in the coprecipitates over the range of Ni/Al ratios used in this study.

The composition of the next nearest neighbor peak gives information on cation distribution in the brucite-type layers. An increase of the coprecipitate aluminum content has a decreasing effect on the next nearest neighbor peak height; see Fig. 3. Thus the contribution of both nickel and aluminum backscatterers must be taken into account in the analysis of the peak composition. The amplitude and phase information for the Ni–Ni and Ni–Al systems have been extracted from the spectra of reference compounds. A well-crystallized $Ni(OH)_2$ and

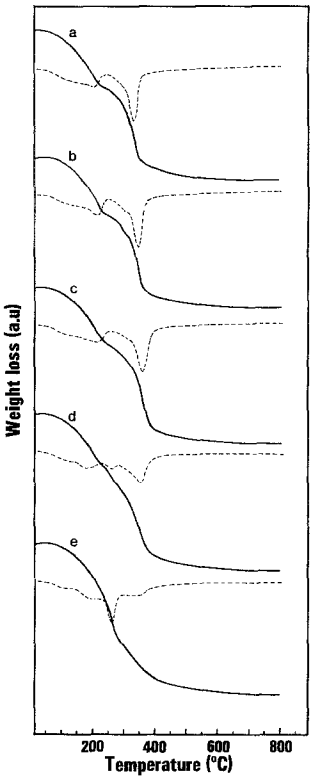

FIG. 2. TG (solid lines) and DTG (dotted lines) of nickel–aluminum mixed hydroxides with different Ni/Al molar ratios after hydrothermal treatment: (a) Ni/Al = 3; (b) Ni/Al = 2.5; (c) Ni/Al = 2.0; (d) Ni/Al = 1.0; (e) Ni/Al = 0.33.

$Ni(OH)_2$ diluted in $Mg(OH)_2$ have been chosen as Ni–Ni and Ni–Al absorber–scatterer pair reference materials, respectively. For the latter reference material, it should be noted that $Ni(OH)_2$ and $Mg(OH)_2$ are completely miscible and that Mg and Al masses are very close (*24*). Furthermore, the structure of the brucite-type layered references is very similar to that of samples A–E. Hence these references are well suited for the EXAFS analysis of nickel–aluminum coprecipitates. The difference between the nickel and aluminum atomic numbers is high enough to distinguish aluminum from nickel retrodiffusor contributions by EXAFS spectroscopy. The best fits of the next nearest neighbor peak composition in samples A–E

TABLE 3

Structural Parameters of Samples A–E Determined by EXAFS Spectroscopy at the Ni *K* edge

Sample	Shell atom	Distance (Å)	Number	σ (Å)	Q	Ni/Al[a]
A	O	2.08	6.3	0.08	0.0086	
	Ni	3.07	5.1	0.09	0.0080	3.2
	Al	3.14	1.6	0.08		
B	Ni	3.07	4.9	0.09	0.0170	2.7
	Al	3.16	1.8	0.07		
C	Ni	3.07	4.6	0.09	0.0170	2.3
	Al	3.12	2.0	0.07		
D	Ni	3.07	4.5	0.09	0.0120	2.3
	Al	3.12	2.0	0.07		
E	Ni	3.07	4.5	0.09	0.0080	2.3
	Al	3.12	2.0	0.07		

Note. The best fits are obtained by minimizing the agreement factor $Q \cdot \Gamma = 1.0$ Å^{-2} for all samples.

[a] As determined from EXAFS measurements.

are listed in Table 3. The precision on the nickel and aluminum numbers is ±0.4. The total next nearest neighbor number is 6.7 ± 0.8 for all samples. This value is compatible with a brucite-type structure for the precipitates. The contribution of the interlayer carbonate ions, such as that of nickel backscatterers belonging to other layers, is negligible. For samples A–C, the Ni/Al ratio determined by EXAFS spectroscopy is slightly higher than that given by X-ray fluorescence but the agreement, taking into account the precision of the nickel and silicon

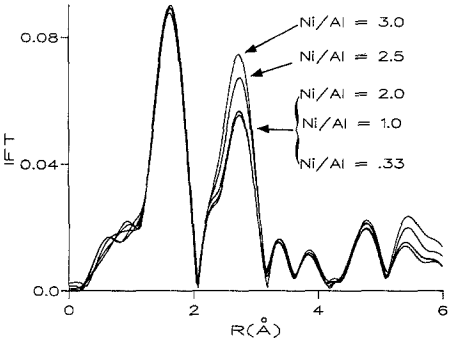

FIG. 3. Fourier-transformed EXAFS spectra (k^3 weighted; without phase correction) of the precursors after hydrothermal treatment.

scatterer numbers, is correct. By contrast, for samples D and E the local environment around Ni(II) ions is exactly the same as that found in sample C; see Table 3 and Fig. 3. Thus the EXAFS spectroscopy shows that for Ni/Al atomic ratios lower than 2 the coprecipitation leads to the mixture of, first, a hydrotalcite-type mixed hydroxide with a Ni/Al atomic ratio equal to 2 and, second, a Ni-free precipitate likely of aluminum hydroxide or oxyhydroxide nature. This conclusion agrees well with the XRD analysis.

In conclusion, the repartition of Ni(II) and Al(III) ions in samples A–C is found to be very homogeneous. In particular, no segregation of aluminum hydroxide takes place in these samples. Conversely, the coprecipitation does not lead to a single phase product for Ni/Al atomic ratios lower than 2, the formation of aluminum oxyhydroxide being revealed by X-ray diffraction and confirmed by thermogravimetric and EXAFS analysis. In this case, a subsequent calcination will probably lead to the formation of an alumina phase in addition to the products of decomposition of the hydrotalcite phase. One goal of this study is the characterization of a Ni-doped alumina phase among the products of decomposition of the nickel–aluminum hydrotalcite-type precipitates: the samples D and E have thus been excluded from the following characterization of the calcined precursors.

Characterization of the Calcined Precursors

The XRD patterns of the precursors heated in air at various temperatures have been previously examained (*9, 21, 23*). The main results are: first, the only phase detected from 350 to 800°C is NiO. The NiO crystallite size increases slightly with the calcination temperature, showing a high thermal stability; see Table 4. No alumina phase is detected. Second, the nickel oxide lattice parameters are lower than those of pure nickel oxide, suggesting the presence of Al(III) ions inside the NiO particles. Third, the spinel-phase $NiAl_2O_4$ pattern is observed only when the calcination temperature reaches 850°C (*21*). Simultaneously the NiO average crystallite size undergoes a very fast increase, indicating a complete separation of NiO and $NiAl_2O_4$ phases.

The Fourier-transformed EXAFS spectra at the Ni *K* edge of sample B calcined at 350, 450, and 650°C are presented in Fig. 4 with that of bulk NiO. The presence of nickel oxide particles in sample B calcined at 350°C is revealed by the characteristic features of NiO spectrum between 2 and 6 Å. The height of the next nearest neighbor peak increases with calcination temperature: this fact is consistent with XRD data indicating an increase of the NiO particle sizes with calcination temperature (see Table 4). The determination of NiO particle sizes by EXAFS is in progress. This study should give more insight on the possible presence of other Ni-containing phases in addition to NiO.

The specific surface areas of sample B calcined at various temperatures are reported in Table 4. There is a marked decrease of the surface area for calcination above 900°C, in accord with previous work (*13*).

In order to separate nickel oxide from aluminum-rich phases, washing of calcined precursor with various acidic and alkaline solutions was performed. The calcined products were found to be completely soluble in acidic solutions. By contrast, a treatment in basic solutions did not affect the nickel oxide particles, whereas, significant amounts of aluminum ions were removed by dissolution into the liquid phase.

Treatment of Calcined Precursors by Hot Concentrated Sodium Hydroxide Solutions

As the results for all samples A, B, C are identical, further discussion is limited to sample B. The Al(III) concentration in the washing solutions as a function of washing time for sample B calcined at 450 and 650°C is presented in Fig. 5. The Al(III) concentration in the solution was found to rapidly

TABLE 4

Composition, Specific Surface Area, and XRD Data of Sample B Calcined and NaOH treated

Calcination temp (°C)	NaOH treatment	Water rinsing	Recalcination temp (°C)	Ni/Al molar ratio	Surface area (m^2/g)	Phases identified by XRD	NiO crystallite size (nm)	NiO lattice parameter a (nm)
450	No	—	—	2.5	219	NiO	3.5	0.4154(5)
650	No	—	—	2.5	147	NiO	5.5	0.4165(3)
750	No	—	—	2.5	130	NiO	7.0	0.4178(2)
900	No	—	—	2.5	27	NiO + $NiAl_2O_4$	>50	0.4176(2)
650	Yes	No	—	6.5	n.d.	NiO + $Ni(OH)_2$ Hydrate[a]	5.0	0.4173(3)
650	Yes	Yes	120	6.5	n.d.	NiO	5.0	0.4174(3)
650	Yes	Yes	650	6.5	96	NiO	5.7	0.4181(3)

Note. Lattice parameter of pure NiO according to JCPDS 04-0835: 0.4177 nm. n.d., not determined.
[a] See JCPDS 38-0715.

reach a plateau (135 mg/liter for sample B calcined at 650°C; see Fig. 5). By contrast, the Ni(II) concentration in the washing solutions was always very low, around 0.5–2 mg/liter for all samples. This low concentration may be related to the low solubility of $Ni(OH)_2$ at pH 14 in the absence of ammonia (*27*): the precipitation of nickel hydroxide during the NaOH treatment cannot be excluded. The quantity of Al(III) ions remaining in the washed mixed oxide was found to be independent of the volume of washing solution.

The maximum concentration of Al(III) ions in solution, obtained after 2 h washing, as a function of the calcination temperature of the precursor is presented in Fig. 6. The solubility of the dried precursor is very low, such as that of nickel hydroxide. Likewise, the precursor calcined at 850°C, consisting

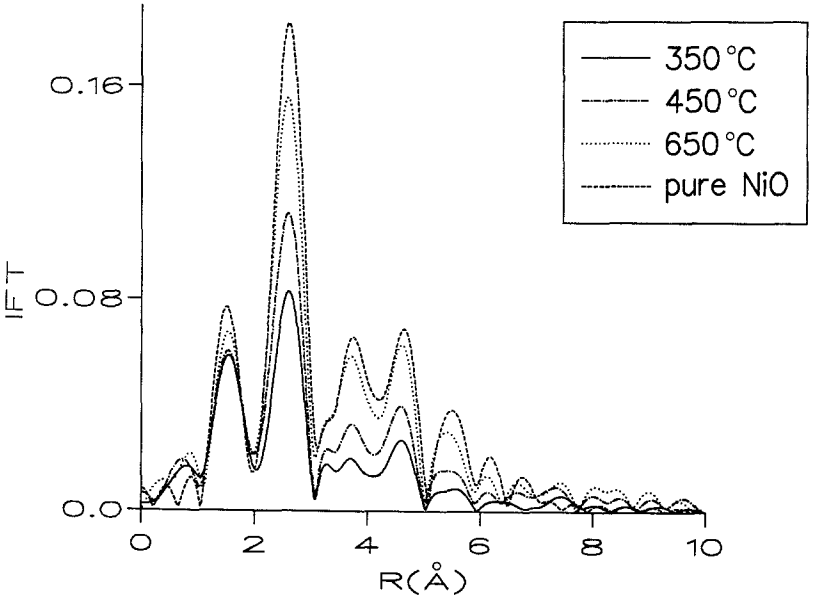

FIG 4. Fourier-transformed EXAFS spectra (k^3 weighted; without phase correction) of sample B calcined at 350, 450, 650°C, and of bulk NiO.

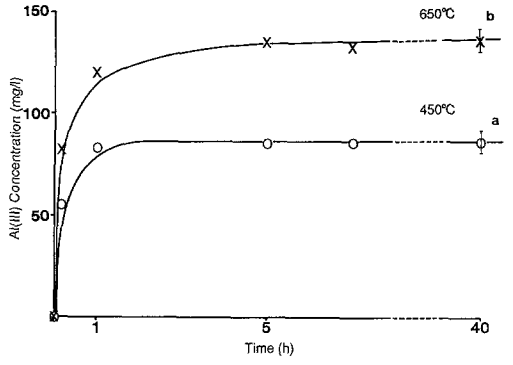

FIG. 5. Al(III) ion concentration in washing solution as a function of NaOH treatment time; (a) sample B calcined at 450°C; (b) sample B calcined at 650°C. 0.2 g of calcined precursor was washed in 0.1 l of molar sodium hydroxide solution. The calculated Al(III) ion concentration corresponding to the total oxide dissolution is 227 mg/liter.

of large crystallites of nickel aluminate and nickel oxide, has a very low solubility in basic medium. The amount of Al(III) that passed in solution exhibits a maximum for calcination temperatures around 700°C: 60% of aluminum initially present in the calcined precursor was dissolved.

Electron micrographs of sample B before and after calcination at 650°C are shown in Fig. 7 and 8 and a micrograph of sample B after NaOH treatment in Fig. 9. The morphology of sample B is characteristic of a hydrotalcite-type precursor (*25, 26*), with platelets about 20 to 60 nm in size. After calcination at 650°C, the general morphology is conserved but with a nodular appearance, see Fig. 8. These nodules are about 5 nm in size and are probably the NiO particles revealed by the XRD analysis. The nodules seem to be embedded in another phase. The same description is valid for the material washed with NaOH; see Fig. 9. In addition to this morphology, however, highly contrasted large particles are observed. These particles may arise from nickel hydroxide reprecipitation during washing. To verify this hypothesis, the sample was rinsed with distilled water until these large particules were no longer observed. The XRD patterns of sample B calcined at 650°C before and after washing with sodium hydroxide solution and the XRD pattern of the latter after subsequent rinsing with distilled water are presented in Fig. 10. The hydrated $Ni(OH)_2$ structure visible in Fig. 10b in addition to that of NiO has disappeared after rinsing with distilled water. Furthermore, the atomic Ni/Al ratio in the contrasted particles given by X-ray microanalysis (STEM) was found to be higher than 100: the particles were not of hydrotalcite type. Thus the hypothesis of reprecipitation of nickel hydroxide during treatment with sodium hydroxide solution is confirmed. The particles of nickel hydroxide are simply deposited onto the NaOH-treated mixed oxides; they are removed by a subsequent rinsing with distilled water. The Ni/Al ratio in the samples measured by X-ray fluorescence is not modified by rinsing; see Table 4. Thus the amount of Ni(II) in the nickel hydroxide particles in comparison with the total amount of Ni(II) in the samples is small.

The XRD data relative to the NaOH treated mixed oxides without subsequent calcination are reported in Table 4. The NiO crystallite sizes are not modified. The NiO particles do not appear to be altered by the NaOH treatment. On the other hand, the NiO lattice parameter increases and becomes very close to that of pure NiO.

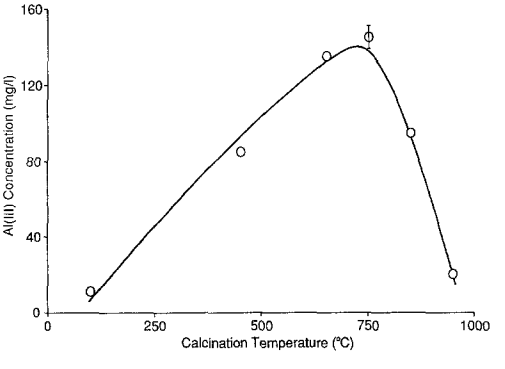

FIG. 6. Al(III) ion concentration in washing solution as a function of the calcination temperature of the precursor. The calculated Al(III) ion concentration corresponding to the total oxide dissolution is 227 mg/liter.

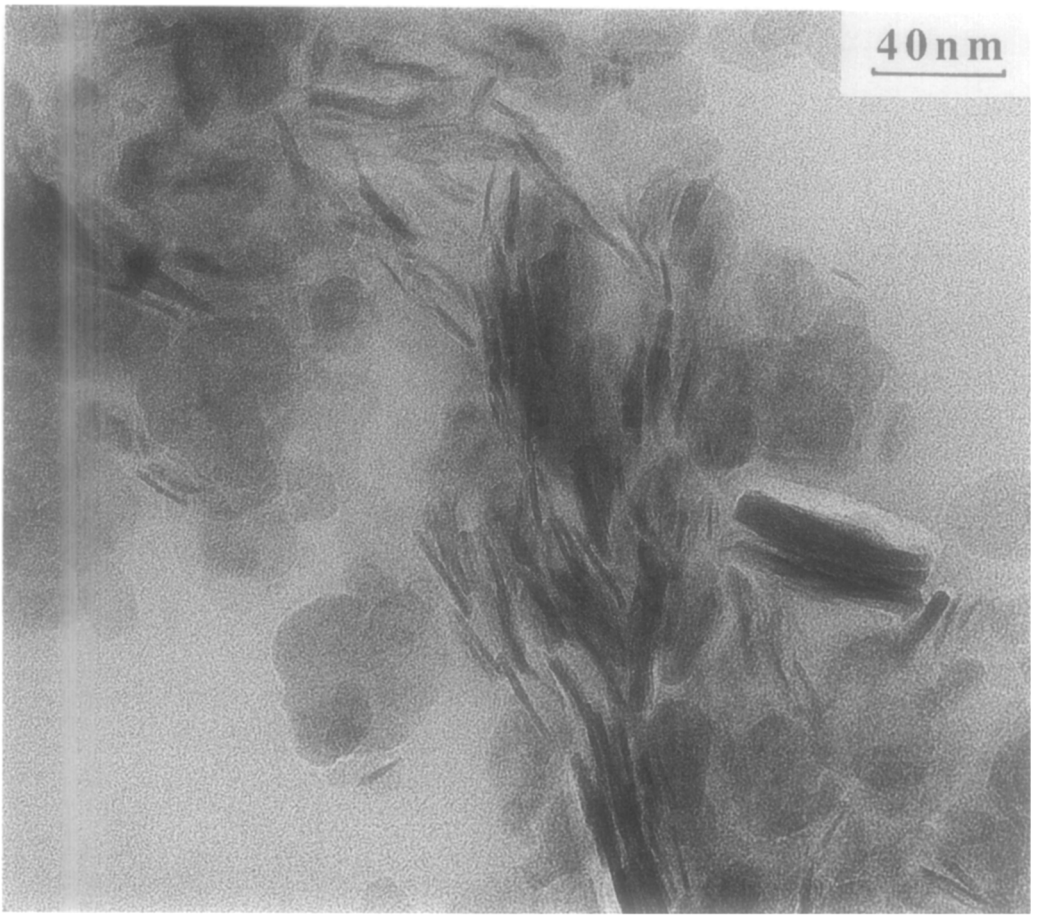

FIG. 7. Electron micrograph of sample B before calcination.

Large particles of nickel hydroxide deposited on mixed oxides form large NiO particles upon calcination, which alters the interpretation of the NiO average crystallite size from XRD data. It is therefore important to rinse the samples before further analysis.

Thermal Properties of the NaOH Treated, Rinsed, Calcined Precursors

The thermal stability and reducibility of the calcined precursors after NaOH treatment and water rinsings have been investigated.

The lattice parameters and crystallite sizes of NiO particles in the NaOH-treated samples after subsequent calcination are presented in Table 4. The lattice parameters are very close to those of pure NiO. The NiO crystallite sizes are the same in the treated and in the untreated materials after calcination at the same temperature; see Fig. 11. Thus the removal of more than one-half of the Al(III) ions initially present in calcined materials has no effect on the thermal stability of the NiO particles.

The specific surface areas of sample B calcined at 650°C and of the latter sample NaOH-treated, water-rinsed then recalcined at 650°C are reported in Table 4. The NaOH treatment results in a decrease in area of 30%.

The TPR profiles of (a) sample B calcined at 650°C and (b) sample B calcined

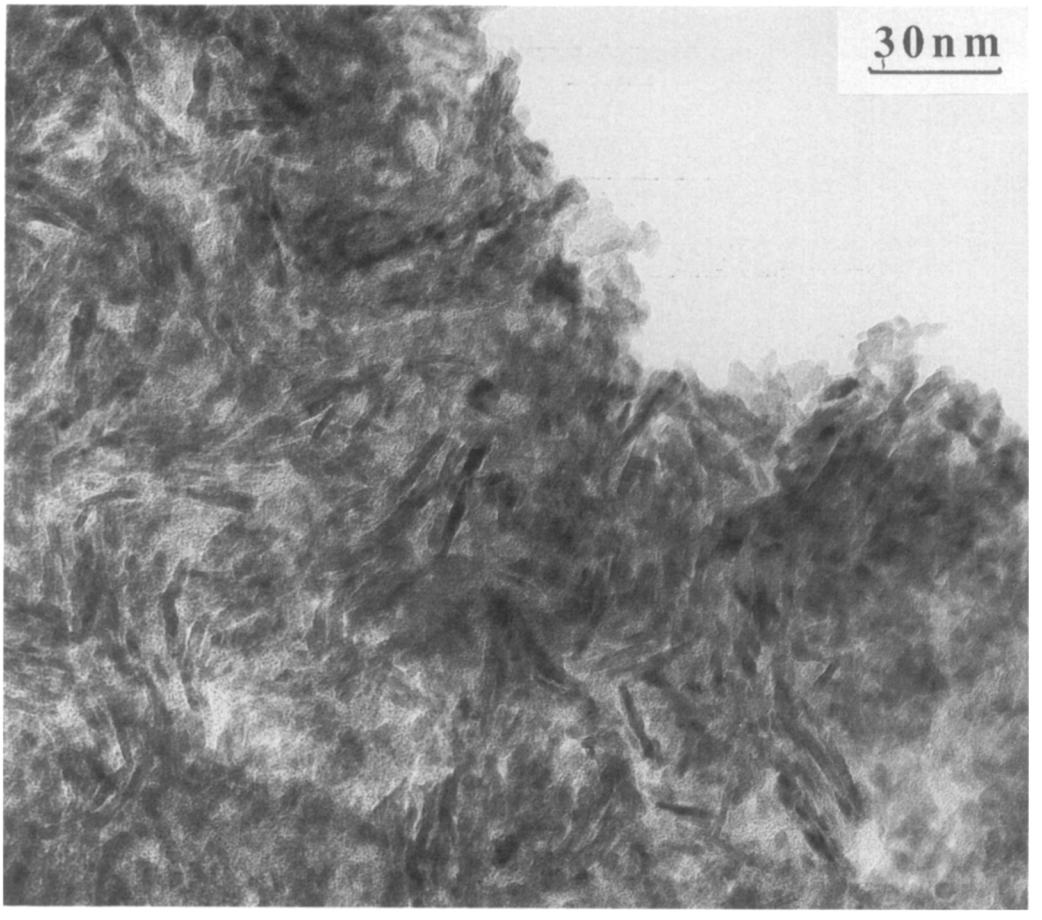

FIG. 8. Electron micrograph of sample B calcined at 650°C.

at 650°C then washed and calcined at 650°C are presented in Fig. 12. The treatment with sodium hydroxide solution involves a slight increase of the NiO particle reducibility, the reduction starting at lower temperatures. Nevertheless, the maximum of the hydrogen consumption profile is not modified.

In conclusion, the Al-rich phase, which can be removed by the NaOH treatment, has little influence on the thermal stability and reducibility of the NiO particles, but contributes around 30% to the specific surface area of the calcined precursors. The aluminum fraction remaining in the samples after NaOH treatment is responsible for the thermal properties of the NiO phase.

DISCUSSION

This paper focuses on the characterization of the products of decomposition of nickel–aluminum hydrotalcite-type precursors heated in air. The thermal stability of the obtained NiO particles is well known; however, the location of the Al(III) ions, which are clearly responsible for this interesting property, remains uncertain. The X-ray diffraction analysis of precursors calcined between 300 and 850°C does not reveal phases other than NiO, such as alumina or spinel-type phases, whereas the characteristic reflections of NiO are shifted towards 2θ values higher than those corresponding to pure NiO. The shift of the NiO reflections

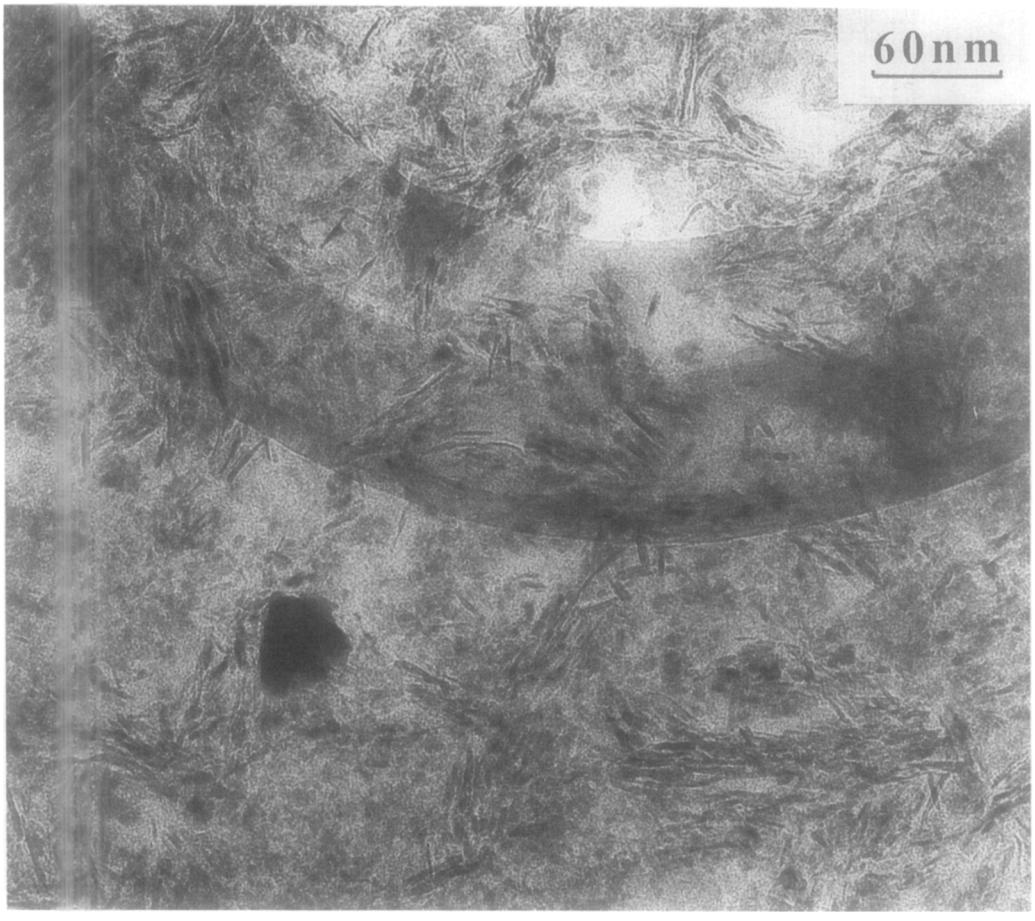

FIG. 9. Electron micrograph of sample B calcined at 650°C then treated with a 1 *M* NaOH solution

may be attributed to the presence of Al(III) ions in the NiO lattice, keeping in mind that the accurate determination of lattice parameters for poorly crystallized materials, such as the samples reported in this study, is very difficult. For samples calcined at temperatures higher than 700°C, however, the NiO lattice distortion becomes negligible (see Table 4). Thus the presence at these calcination temperatures of X-ray amorphous phases containing Al(III) ions located outside the NiO particles is highly probable.

The study of the reducibility of the NiO particles as a function of the calcination temperature also provides interesting information on phase composition in calcined hydrotalcite-type precursors. The TRP profiles of the calcined precursors have already been presented by us and others (*10, 21*). One broad peak only is observed for the samples calcined up to 900°C. This suggests that NiO is the main nickel-containing phase in the mixed oxides. The reduction peak shifts toward high temperatures as the calcination temperature increases. The hindered reducibility in comparison with unsupported nickel oxide is obviously related to the presence of Al(III) ions in the mixed oxides, which may be present in the nickel oxide lattice or in another phase strongly interacting with nickel oxide. The former hypothesis is not consistent with XRD data, since the NiO phase becomes more difficult to reduce when the calcination temperature

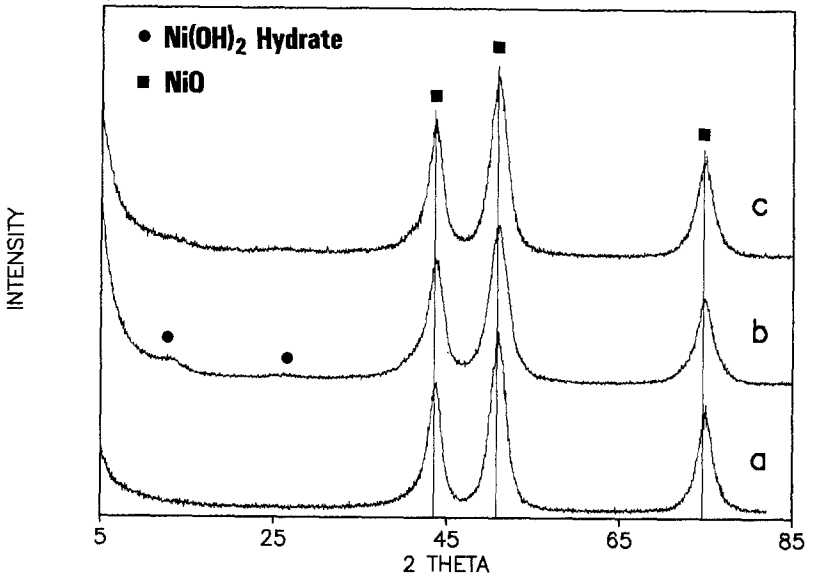

FIG. 10. XRD patterns of (a) sample B calcined at 650°C; (b) (a) after NaOH treatment; (c) (b) after rinsing with distilled water.

increases, although the NiO lattice parameters shift toward those of pure nickel oxide. Thus there are doubts that the presence of Al(III) ions inside the nickel oxide particles is responsible for the low reducibility of NiO in calcined samples.

Hence both XRD analysis and TPR investigation strongly suggest that the thermal

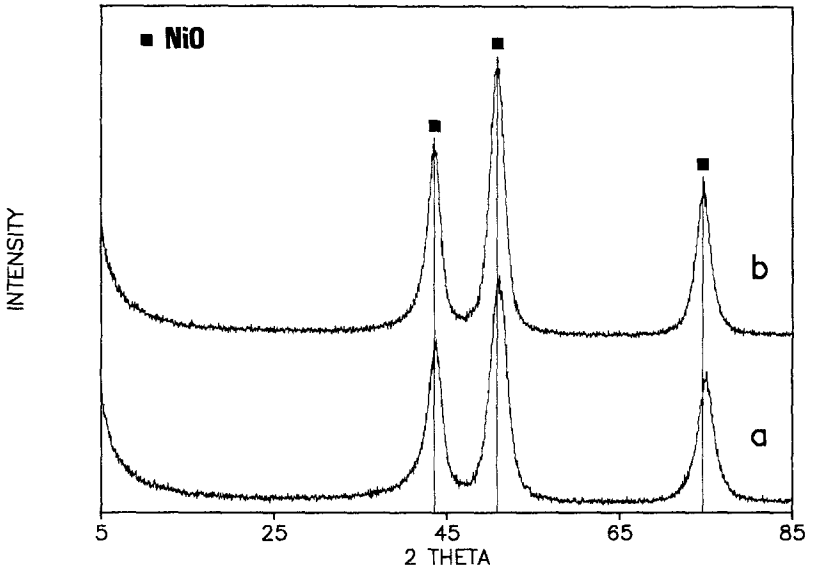

FIG. 11. XRD patterns of (a) sample B calcined at 650°C; (b) (a) after NaOH treatment; rinsing, then calcination at 650°C.

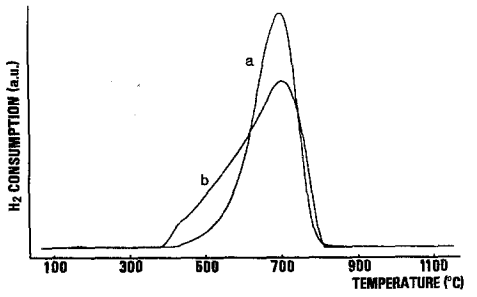

FIG. 12. Temperature-programmed reduction profiles of (a) sample B calcined at 650°C; (b) (a) treated with 1 *M* NaOH, rinsed with distilled water, then calcined at 650°C.

properties of the nickel oxide phase cannot be explained by the presence of Al(III) ions inside the NiO particles. Aluminum-rich phases are likely present in the calcined precursors. These phases are X-ray amorphous and contribute to the low reducibility of the NiO particles. They may also contribute to the thermal stability of the nickel oxide phase: therefore we attempted to separate nickel oxide and other Al-rich phases by selective dissolution in various media. Acidic solutions are aggressive for NiO-, alumina-, spinel-, or hydroxide-type phases: thus the treatment in acidic medium is not selective enough. By contrast, the solubility of NiO and $Ni(OH)_2$ is known to be very low in strongly basic media (*27, 28*) whereas alumina phases dissolve more easily in these conditions.

When calcined precursors are treated in sodium hydroxide solutions, an important fraction of Al(III) ions initially present in the samples goes into solution. This fraction does not depend on the volume of NaOH solution used for washing. Thus there is no chemical equilibrium, such as a solubility equilibrium for example, between the Al(III) concentration in solution and the undissolved Al(III) fraction in the solid. Likewise, the Na concentration measured by X-ray fluorescence analysis is found to be negligible in the washed mixed oxides: thus the NaOH treatment does not involve the exchange of Al^{3+} by Na^+ cations in the calcined precursors. The Ni–Al mixed oxides obtained from hydrotalcite decomposition do not exhibit microporosity: the pore size distribution of Ni–Al hydrotalcites calcined at 650°C show one peak at approximately 6 nm (*21*). Hence the aluminum removal by NaOH treatment is very different from framework dealumination of zeolites by acid leaching. The nickel oxide, like magnesia, has the NaCl structure (*29*). However, the rehydration of nickel oxide to nickel hydroxide is much more difficult than that of magnesia: indeed, the XRD pattern of sample B after NaOH treatment and water rinsing only presents the NiO reflections; see Fig. 10c. It is very unlikely that the NiO particles form nickel hydroxide first, the Al fraction initially included inside the NiO particles being removed by dissolution in NaOH solution, and the nickel hydroxide then forms NiO particles of the same size again! The deposition after NaOH treatment of large nickel hydroxide particles weakly bound to the samples suggests that an aluminum- and nickel-containing phase has dissolved. The Al(III) ions form hydrated aluminate ions in NaOH solution (*30–32*), whereas the Ni(II) ions reprecipitate onto the washed samples. The amount of Ni(II) in the deposited $Ni(OH)_2$ particles with respect to the Ni(II) amount in the sample is low and not detectable by X-ray fluorescence, whereas the amount of removed aluminum is between 40 and 60% of the aluminum initially present in the samples. Thus it is likely that the phase that enters in solution is a Ni-doped alumina. This phase is responsible for the shift of the NiO reflections observed in the XRD pattern of the calcined materials, since this shift is canceled by the NaOH treatment. For calcination temperatures about 650–750°C, the aluminum fraction contained in the alumina phase is around two-thirds of the aluminum present in the samples; see Fig. 6 and Table 4. The contribution of the alumina phase to the specific surface area of the samples calcined at 650°C is little more than 30%.

The formation of the alumina phase upon calcination does not arise from the existence of a Ni-free or Ni-doped aluminum (oxy)hydroxide phase in the precursor, since the hydrotalcite-type precursors were found to be very homogeneous. Therefore we have moved aside nonhomogeneous mixed hydroxides obtained for Ni/Al atomic ratios lower than 2. The results concerning the precursors are consistent with previous work (*22*). Ni(II) and Al(III) cations are homogeneously distributed in brucite-type layers (hydrotalcite-type structure) when the Ni/Al atomic fraction in the coprecipitates ranges from 2 to 3. The separation of an aluminum hydroxide or oxyhydroxide phase from the hydrotalcite phase occurs in the precipitates after hydrothermal treatment for Ni/Al atomic ratios lower than 2 (samples D and E). The structure of the coprecipitates deduced from X-ray diffraction and thermal analysis is confirmed by EXAFS spectroscopy. EXAFS is shown to be a useful tool to ensure that no separation of discrete aluminum or nickel hydroxide phases occurs during coprecipitation. EXAFS at the Ni *K* edge provides information on the possible formation of an aluminum (oxy)hydroxide phase. Likewise, EXAFS at the Al *K* edge should give information on the segregation of a nickel hydroxide phase; this work is in progress and will be presented in a future paper. In short, even though samples D and E were not calcined and further investigated, initial studies of these precursors have proven that the TG and EXAFS techniques can accurately distinguish between heterogeneous and homogeneous precursors.

The Al(III) ions remaining in the NaOH-treated materials cannot be extracted by the NaOH treatment. This aluminum fraction is, however, of paramount importance for the thermal stability of the mixed oxides. The remaining Al(III) ions may be included inside the lattice of the nickel oxide particles, as was suggested for the unwashed mixed oxides. However, the NiO lattice distorsion after NaOH treatment is found to be negligible; see Table 4. Thus it seems more likely that the remaining Al(III) ions form another phase outside the NiO particles and in strong interaction with them. This phase constitutes the true support for nickel oxide and is responsible for the thermal properties of the calcined NiAl hydrotalcites. By analogy with previous studies concerning alumina-supported catalysts (*33, 34*), a spinel-type structure may be hypothesized, the formation of $NiAl_2O_4$ being reported at temperatures as low as 650°C by many authors (*12, 35–38*). However, we have already observed that the formation of true spinels had a detrimental effect to the thermal stability of nickel–chromium and nickel–aluminum mixed oxides (*21*). For calcination temperatures above 900°C, Ni Al_2O_4 formation is revealed by X-ray diffraction whereas both NiO crystallite size and reducibility markedly increase. Thus the "spinel-type" phase consists of a nonstoichiometric, very poorly crystallized phase. The Al(III) ions may also be retained in partially decomposed brucite-type platelets. The compensation for the excess charge in the brucite-type layers in the absence of carbonate ions may be satisfied by cation vacancies in the layers, as already proposed for nickel hydroxide (*39*). In fact, the determination of the exact nature of this Al-containing phase is very difficult: no phase other than NiO is revealed by XRD; the ^{27}Al NMR spectra are broadened beyond detection by the paramagnetic Ni(II) species. An EXAFS investigation of NaOH-treated samples at the Al *K* edge should give more insight on the Al environment and will be presented in a further paper.

We may now present a model for the thermal decomposition of Ni–Al hydrotalcite-type precursors consistent with our observations and previous studies. In the precursors, the Ni(II) and Al(II) cations are homogeneously distributed in brucite-type layers for Ni/Al atomic ratios between 2 and 3. As mentioned in previous work (*13*), there is no relationship between the particle size of the coprecipitates and that of the NiO parti-

cles formed upon calcination. The hydrothermal treatment has no influence on the thermal properties and crystallite sizes of the oxidic form of the materials. The Ni–Al hydrotalcite decomposition proceeds topotactically, as reported previously for Mg–Al hydrotalcites (*23, 40*). The general morphology is conserved upon calcination, although the composition of the mixed oxides varies locally, as suggested in this study. The thermal decomposition of the Ni–Al hydrotalcites leads to the segregation of three phases: a NiO phase, a Ni-doped Al_2O_3, and a spinel-type compound. The alumina phase can be readily removed by NaOH leaching. This phase contributes little to the nickel oxide stability. The spinel-type phase plays a major role in the thermal properties of the mixed oxides and may be visualized either as decorating the NiO particles or as acting as a support for the NiO particles. The thermal sintering of the NiO phase is thus avoided. Likewise, the reduction of the NiO particles is strongly hindered by the presence of the spinel-type phase at the surface of the particles, making the generation of nickel nuclei at the NiO surface difficult. This conclusion is quite similar to that of a previous work of Ross *et al.* (*41*) concerning alumina-supported nickel catalysts. The spinel-type phase also protects the alumina phase against crystallization. This phase likely plays an important role for the stability of the reduced catalysts, preventing nickel particles from sintering.

The nonhomogeneity of the mixed oxides obtained from decomposition of hydrotalcite type precursors illustrates the limits to the use of foreign ions (here Al(III) ions) to stabilize the crystallite sizes and specific area of oxides. The nickel oxide phase obtained by calcination of Ni/Al hydrotalcites exhibits a high thermal stability in comparison with NiO formed by calcination of nickel hydroxide. Unfortunately, the Al(III) ions are concentrated onto and in the NiO surface, forming other phases such as alumina or spinel-type phases, so that the NiO surface is wholly modified. One-third of the total surface area arises from an alumina phase. The segregation of phases upon calcination of hydrotalcite-type homogeneous precursors may occur in other systems, such as Al(III)-stabilized magnesia. The latter precursors have been used as supports for metallic particles (*42*) and as basic catalysts (*2, 43*). Even though the chemical properties of MgO and NiO are different, the possibility that Mg-doped alumina, magnesium carbonate, and spinel-type phases may coexist with magnesia in such systems should not be overlooked.

ACKNOWLEDGMENTS

We express our thanks to Mmes. Ubrich and Russmann for TGA and TPR measurements, to M. Gueroult for electron micrographs, and to M. Varin for assistance in graphic design. We express our thanks to the LURE staff for help during EXAFS experiments. Stimulating discussions with Dr. C. Cameron are gratefully acknowledged.

REFERENCES

1. Reichle, W. T., US Patent 4,458,026 (1984).
2. Reichle, W. T., *J. Catal.* **94,** 547 (1985).
3. Suzuki, E., and Ono, Y., *Bull. Chem. Soc. Jpn.* **61,** 1008 (1988).
4. Courty, P., Durand, D., Freund, E., and Sugier, A., *J. Mol. Catal.* **17,** 241 (1982).
5. Courty, P., and Marcilly, C., *in* "Preparation of Catalysts III" (G. Poncelet *et al.*, Eds.), p. 485. Elsevier, Amsterdam, 1983.
6. Gherardi, P., Ruggeri, O., Trifiro', F., Vaccari, A., Del Piero, G., Manara, G., and Notari, B., *in* "Preparation of Catalysts III" (G. Poncelet *et al.*, Eds.), p. 723. Elsevier, Amsterdam, 1983.
7. Gusi, S., Pizzoli, P., Trifiro', F., Vaccari, A., and Del Piero, G., *in* "Preparation of Catalysts IV" (B. Delmon *et al.*, Eds.), p. 753. Elsevier, Amsterdam, 1987.
8. Rostrup-Nielsen, J. R., "Steam Reforming Catalysts." Teknisk Forlag, Copenhagen, 1975.
9. Puxley, P. C., Kitchener, I. J., Komodromos, C., and Parkyns, N. D., *in* "Preparation of Catalysts III" (G. Poncelet *et al.*, Eds.), p. 237. Elsevier, Amsterdam, 1983.
10. Ross, J. R. H., "Catalysis, Specialist Periodical Reports," Vol. 7, p. 1. Royal Society of Chemistry, London, 1985.
11. Williams, A., Butler, G. A., and Hammonds, J., *J. Catal.* **24,** 352 (1972).
12. Simonova, L. G., Dzis'ko, V. A., Borisova, M. S., Karakchiev, L. G., and Olenkova, I. P. *Kinet. Katal.* **12,** 157 (1973).

13. Alzamora, L., Ross, J. R. H., Kruissink, E. C., and Van Reijen, L. L., *J. Cham. Soc. Faraday Trans. 1* **77,** 665 (1981).
14. El-Shobaky, G. A., Ghoneim, N. M., and Sultan, E. A., *Thermochim. Acta* **63,** 39 (1983).
15. Hernandez, M. J., Angeles Ulibarri, M. A., Rendon, J. L., and Serna, C. J., *Thermochim. Acta* **81,** 311 (1984).
16. Doesburg, E. B. M., de Korte, P. H. M., Schaper, H., and van Reijen, L. L., *Appl. Catal.* **11,** 155 (1984).
17. Lansink Rotgerink, H. G. J., Bosch, H., van Ommen, J. G., and Ross, J. R. H., *Appl. Catal.* **27,** 41 (1986).
18. Doesburg, E. B. M., Hakvoort, G., Schaper, H., and van Reijen, L. L., *Appl. Catal.* **7,** 85 (1983).
19. Hosemann, R., Preisinger, A., and Vogel, W., *Ber. Bunsenges. Phys. Chem.* **70,** 797 (1966).
20. Schultz, J. M., *J. Catal.* **27,** 64 (1972).
21. Clause, O., Gazzano, M., Trifiro', F., Vaccari, A., and Zatorski, L., *Appl. Catal.* **73,** 217 (1991).
22. Kruissink, E. C., van Reijen, L. L., and Ross, J. R. H., *J. Chem. Soc. Faraday Trans. 1* **77,** 649 (1981).
23. Sato, T., Fujita, H., Endo, T., Shimada, M., and Tsunashima, A., *React. Solids* **5,** 219 (1988).
24. Pascal, P., "Nouveau Traité de Chimie Minérale," Vol. 17, p. 742. Masson, Paris, 1963.
25. Szymanski, R., Travers, C., Chaumette, P., Courty, P., and Durand, D., *in* "Preparation of Catalysts IV" (B. Delmon *et al.*, Eds.), p. 739. Elsevier, Amsterdam, 1987.
26. Thevenot, F., Szymanski, and Chaumette, P., *Clays Clay Miner.* **37,** 396 (1989).
27. "Gmelins Handbuch der Anorganischen Chemie," Vol. 57, pp. 429, 459. Verlag Chemie, Weinheim, 1966.
28. Cotton and Wilkinson, "Advanced Inorganic Chemistry," p. 785. Wiley, New York, 1980.
29. Wells, A. F., "Structural Inorganic Chemistry," p. 538. Clarendon Press, Oxford, 1984.
30. Cotton and Wilkinson, "Advanced Inorganic Chemistry," p. 334. Wiley, New York, 1980.
31. Heslop, R. B., and Robinson, P. L., "Inorganic Chemistry," p. 343. Elsevier, Amsterdam, 1967.
32. Kragten, J., "Atlas of Metal-Ligand Equilibria in Aqueous Solution," p. 53. Wiley, New York, 1978.
33. Bartholomew, C. H., Pannell, R. B., and Fowler, R. W. *J. Catal.* **79,** 34 (1983).
34. Al-Ubaid, A., and Wolf, E. E., *Appl. Catal.* **40,** 73 (1988).
35. Lo Jacono, M., Schiavello, M., and Cimino, A., *J. Phys. Chem.* **75,** 1044 (1971).
36. Dufresne, P., Payen, E., Grimblot, J., and Bonnelle, J. P., *J. Phys. Chem.* **85,** 2344 (1981).
37. Houalla, M., Lemaitre, J., and Delmon, B., *J. Chem. Soc. Faraday Trans. 1* **78,** 1389 (1982).
38. Huang, Y. J., Schwarz, J. A., Diehl, J. R., and Baltrus, J. P., *Appl. Catal.* **36,** 163 (1988).
39. De Roy, A., Besse, J. P., and Bondot, P., *J. Phys.* **47,** C8-713 (1986).
40. Reichle, W. T., Kang, S. Y., and Everhardt, D. S., *J. Catal.* **101,** 352 (1986).
41. Ross, J. R. H., Steel, M. C., and Zeini-Isfahani, A., *J. Catal.* **52,** 280 (1978).
42. Davis, R. J., and Derouane, E. G., *Nature* **349,** 313 (1991).
43. Schaper, H., Berg-Slot, J. J., and Stork, W. H. J., *Appl. Catal.* **54,** 79 (1989).